

The Impact of Ion Migration on the Electro-Optic Effect in Hybrid Organic–Inorganic Perovskites


Meng-Jia Sun, Randy Sabatini, Pei-Xi Wang, Amin Morteza Najarian, Koen Bertens, Andrew Johnston, Sjoerd Hoogland, and Edward H. Sargent*

Electro-optic (EO) modulation allows the conversion of electrical signals to optical pulses and is widely employed in telecommunications and chip-to-chip interconnects. Recently, hybrid organic–inorganic perovskites (HOIPs) have been explored as candidates for EO modulators. To improve the EO performance, it is envisioned that halide doping will lower the symmetry of the crystal, enhancing spontaneous polarization. However, mixed halide perovskites are often associated with ion migration, which may impact their EO properties. Thus, the influence of ion migration on the EO efficiency is investigated using Br-doped Dion–Jacobson quasi-2D HOIPs, (4AMP)(MA)Pb₂(Br_{*x*}/I_{*1-x*})₇ (4AMP = 4-(aminomethyl)piperidinium, MA = methylammonium). While density functional theory predicts a greater spontaneous polarization for the Br-doped sample, it is found that experimental results are affected by ion migration. The EO coefficient of the Br/I mixed sample is 95 pm V⁻¹ at 1 kHz (≈50× higher than the undoped sample), but the response falls off rapidly with frequency. This frequency dependence is correlated with impedance spectroscopy, showing that the large EO signal results from ion migration. This study shows that ion migration impacts the EO analysis of mixed halide perovskites and must be considered in future EO studies.

1. Introduction

Electro-optic (EO) modulators are key components in optical interconnects that convert electrical signals to optical pulses.^[1] The linear EO effect (the Pockels effect) produces a refractive index change proportional to the electric field in non-centrosymmetric media.^[2] Traditionally, EO materials are either bulk inorganic crystals like lithium niobate (LiNbO₃)^[1] or poled organic polymers.^[3] Hybrid organic–inorganic perovskites (HOIPs), however, combine elements of both material classes (i.e., high crystallinity and solution processibility)^[4] and have been demonstrated as promising scaffolds to build EO materials.^[5] In particular, polarized organic ligands, aligned between the interlayer space of 2D and quasi-2D perovskites, can result

M.-J. Sun, R. Sabatini, P.-X. Wang, A. M. Najarian, K. Bertens, A. Johnston, S. Hoogland, E. H. Sargent
Department of Electrical and Computer Engineering
University of Toronto
10 King's College Road, Toronto, Ontario M5S 3G4, Canada
E-mail: ted.sargent@utoronto.ca

 The ORCID identification number(s) for the author(s) of this article can be found under <https://doi.org/10.1002/adfm.202107939>.

DOI: 10.1002/adfm.202107939

in overall spontaneous polarization (P_s),^[6,7] which leads to an EO response.

The general formula for 2D perovskites is A₂BX₄,^[8] where the prototypical example is BA₂PbI₄ (BA = butylammonium). We have recently shown EO modulation from organic perovskites by engineering the A- and B-site cations, respectively.^[9,10] In these cases, the EO response shows significant enhancement either by increasing the molecular dipole moment of the A-site^[10] or by introducing deficiencies in the B-site.^[9] Additionally, halide substitution at the X-site offers a simple method for altering the optoelectronic properties of HOIPs,^[11] as the choice of halide not only impacts the bandgap but also the crystal lattice and structural symmetry.^[12] We envisioned that partial substitution at halide sites would distort the lattice, increasing the overall P_s of the system and thus improving the EO performance.

Halide doping has often resulted in ion migration,^[13,14] which can affect device performance. While ion migration in metal halide perovskites was first reported in 1983,^[15] its impact on optoelectronic devices was not focused on until 30 years later, when anomalous hysteresis was reported in perovskite solar cells.^[16] In the years since, ion migration has become a major focus of the photovoltaic community in the attempt to improve both efficiency and stability of devices.^[17] In addition to photovoltaics, effects of ion migration have also been observed in perovskite light-emitting diodes^[18,19] and photodetectors,^[20] as well as other 2D ferroelectrics.^[21] It is prudent to understand the impact of ion migration on the performance of HOIPs in new applications, such as EO.

In this manuscript, we investigate the impact of ion migration on the EO performance of HOIPs. Specifically, we dope Br into a Dion–Jacobson (DJ) quasi-2D HOIP, (4AMP)(MA)Pb₂(Br_{*x*}/I_{*1-x*})₇ (4AMP = 4-(aminomethyl)piperidinium, MA = methylammonium).^[22a] DJ-type perovskites feature one layer of divalent cations between the inorganic layers, where the long axis of organic cations aligning in an out-of-plane manner is beneficial to build out-of-plane polarization for EO application. Density functional theory (DFT) calculations suggest that the halide doping should result in an increased P_s , compared to the undoped sample, and thus improved EO performance. We find that (4AMP)(MA)Pb₂(Br_{*x*}/I_{*1-x*})₇ exhibits an effective EO coefficient of 95 pm V⁻¹ at 1 kHz (≈50× higher

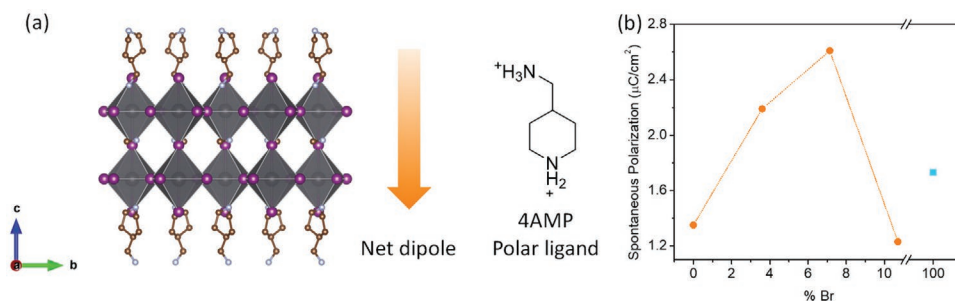


Figure 1. Crystal structure and spontaneous polarization. a) Single crystal structure of 4AMP-I and its net dipole. b) The strength of P_s in doped and undoped crystals calculated by DFT.

than the undoped sample), but the response falls off rapidly with increasing frequencies. We find a similar frequency-dependence using impedance spectroscopy, revealing that the observed EO coefficient is due to ion migration. Our results show that ion migration can impact the EO characterization of perovskites and must be considered in future studies.

2. Results and Discussion

A previous report shows that (4AMP)(MA)Pb₂I₇ (referred to hereafter as 4AMP-I) belongs to the noncentrosymmetric space group (I_a) and has P_s , where all the amino groups of the divalent cations are pointed in the same direction, resulting in a net dipole (Figure 1a), which is the sum of the non-zero dipole moment periodically repeated in every unit cell.^[22] We chose this as a model material to explore the effects of halide doping, with the aim of increased lattice distortion toward a larger EO response. We calculated the P_s of 4AMP-I and mixed-halide (4AMP)(MA)Pb₂(Br_x/I_{1-x})₇ (hereafter 4AMP-Br/I) crystals with different Br-doping ratios, using the Berry phase polarization method based on single crystal X-ray diffraction (XRD) data. The calculations show that the P_s in 4AMP-I is out-of-plane, predominantly perpendicular to the (001) plane (Figure S1 and Table S1, Supporting Information). By doping a small amount of Br ($\approx 7\%$) into the X-site, the P_s is predicted to be twice that of the pure iodide counterpart (Figure 1b and Table S1, Supporting Information). This increase is attributed to the structural distortion and symmetry reduction resulting from substitution with the smaller bromide anion.

We then grew single crystals in an aqueous solution through a step-cooling method (see Experimental Section). This resulted in red crystals with a square, planar shape (Figure S2, Supporting Information). The experimental powder XRD patterns match well with the simulated data from the single crystal structure^[22] of 4AMP-I (Figure S3a, Supporting Information), which confirms that both the doped and undoped crystals are in the same phase. The main peaks in the XRD profiles of 4AMP-Br/I are shifted slightly to higher angles, owing to the Br⁻ doping into the lattice, which decreases the lattice size. The crystal planes were determined by powder XRD, where the free-standing single crystal was placed directly onto the sample holder and measured without grinding (Figure S3b, Supporting Information). The large square planar surface is the (00k) plane and the edge surface is attributed to the (0k0) plane. The different XRD profiles in different directions confirm the highly

oriented crystal structure. Additionally, X-ray photoelectron spectroscopy (XPS) measurements show that there is 6.7% Br-doping (Figure S4 and Table S2, Supporting Information).

Under illumination with a femtosecond laser, both second harmonic generation (SHG) and third harmonic generation signals were observed at room temperature for 4AMP-I and 4AMP-Br/I, with the observed signals tracking the harmonics of the different excitation wavelengths (Figure S5, Supporting Information). The SHG signal confirms their noncentrosymmetric structure and second-order optical nonlinearity. Additionally, angle-resolved Raman spectroscopy was performed to characterize the structural anisotropy of the crystals, with scattered light detected for polarizations parallel or perpendicular to that of the incident light (Figure 2). For angular dependence, we rotated the single crystal, which was placed on either its front facet or an edge facet for in-plane or out-of-plane measurements, respectively. A Raman spectrum (Figure 2b) was taken every 15°. Figure 2c shows the angle-dependent Raman intensity for the parallel configuration, when the 4AMP-Br/I crystal is placed on its edge facet. This results in a 2-lobed shape, with two angles of maximum intensity. This intensity dependence confirms the anisotropy in the out-of-plane direction. The perpendicular configuration exhibits a four-lobed shape (Figure 2d), but its angular dependence is insensitive to anisotropy. See Note S1, Supporting Information, for more details. Similar results were obtained for 4AMP-I (Figure S6, Supporting Information).

To measure the EO response, we used the Teng–Man technique^[23] in transmission mode^[24] by measuring the polarization change of a laser beam transmitted through the crystal as a function of applied electric field (Figure 3a). Briefly, the laser beam at 1550 nm is linearly polarized at 45° with respect to the incident plane, supplying equivalent s- and p-polarization. The crystal's (001) axis, which points in the direction of polarization, is perpendicular to the top surface, confirmed via X-ray diffraction (Figure S3, Supporting Information). The crystal is contacted with a pair of indium tin oxide (ITO) electrodes that apply an electric field along the (001) axis, inducing a refractive index change in this direction. To prevent current flow, an insulating layer of Al₂O₃ (≈ 60 nm) is used on the surface of the ITO electrodes. The transmitted light is sent through a Soleil–Babinet compensator to tune phase retardation between the parallel and perpendicular components. The light is then transmitted through an analyzer before it is finally detected by a Ge near-infrared photodetector connected to a lock-in amplifier.

The EO effect is given by the linear change of the refractive index with an applied alternating electric field, E :

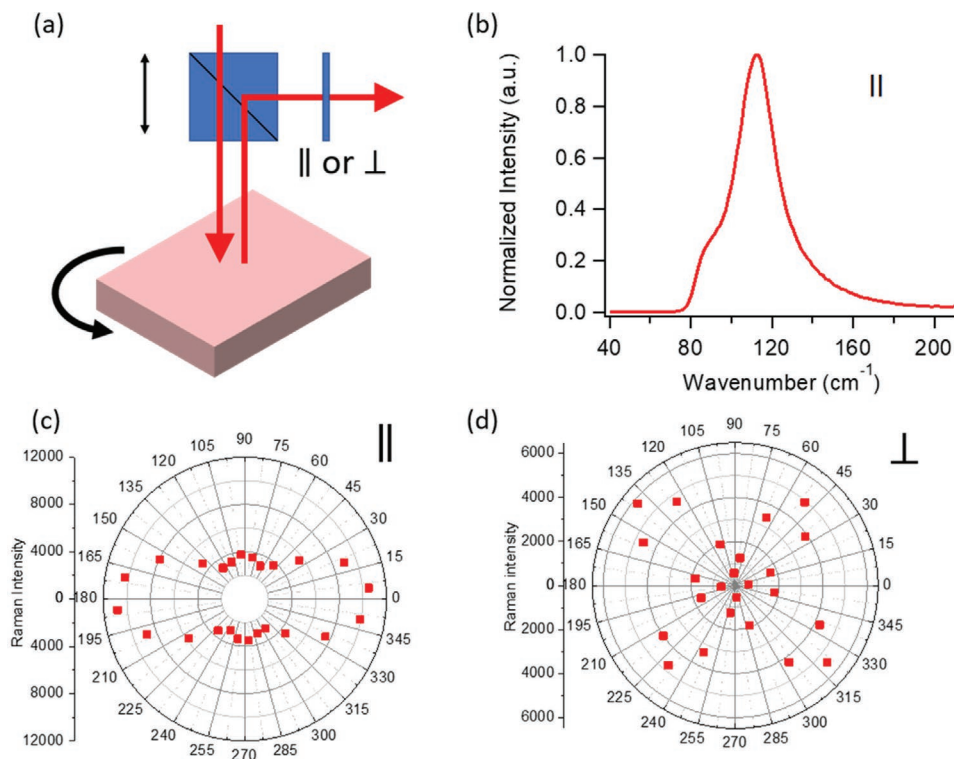


Figure 2. Angle-resolved Raman spectroscopy. a) Schematic of polarized Raman measurements. b) Representative Raman spectrum of 4AMP-Br/I on its edge facet, in the parallel configuration. c) Raman intensity of 4AMP-Br/I on its edge facet, as a function of incident angle, in the parallel configuration. d) Raman intensity of 4AMP-Br/I on its edge facet, as a function of incident angle, in the perpendicular configuration.

$$\Delta n = \frac{1}{2} r_e n^3 E$$

where r_e is the EO coefficient under a certain electric field. We estimated the refractive index of the perovskite (1.8) based on

(1) a previous report.^[25] The r_e was then calculated with the following equation:

$$r_e = \frac{\lambda I_{ac}}{\pi V_{ac} I_c n^2} \frac{(n^2 - \sin^2 \theta)^{3/2}}{(n^2 - 2 \sin^2 \theta)} \frac{1}{\sin^2 \theta} \quad (2)$$

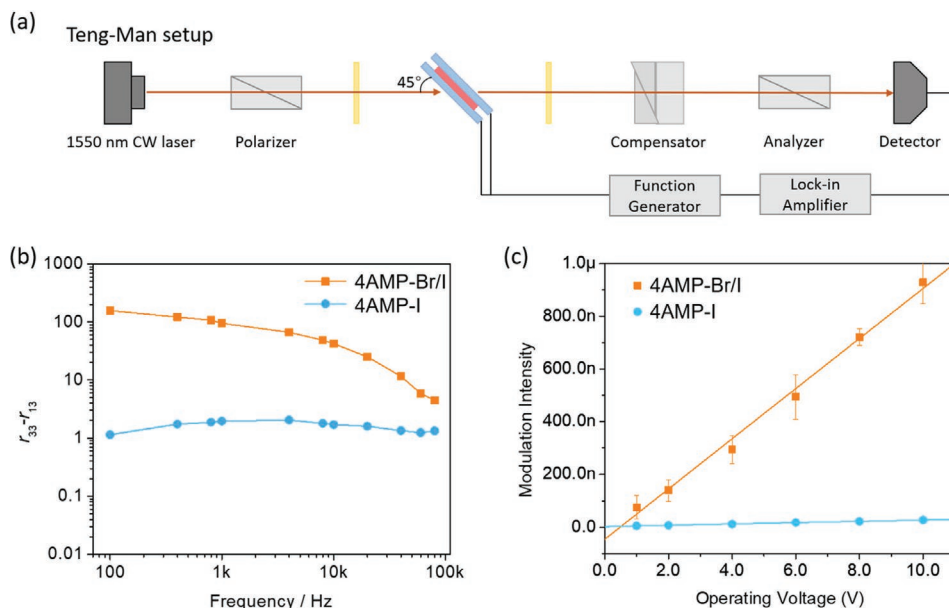


Figure 3. Linear electro-optic effect characterization. a) Schematics of the experimental setup (Teng–Man method). b) EO coefficient as a function of modulation frequency for doped and undoped perovskite crystals. c) The linear growth of the transmitted light power increasing with the operating voltage.

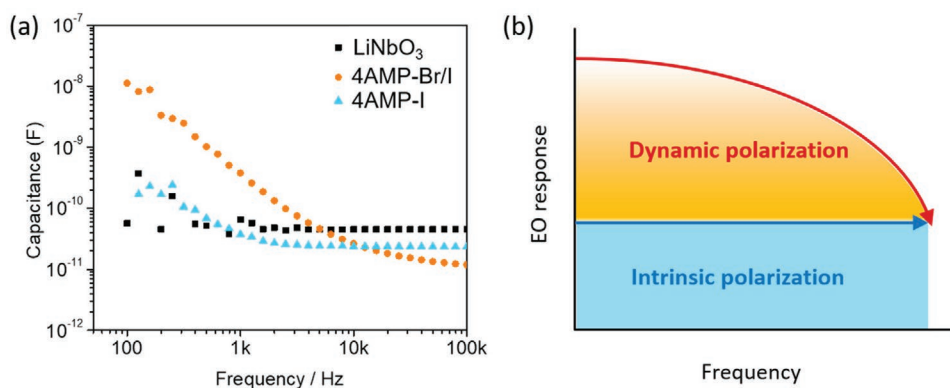


Figure 4. Ion migration characterization in perovskite materials. a) Impedance spectra of LiNbO₃, 4AMP-I, and 4AMP-Br/I single crystals. b) Schematic of frequency-dependent EO response.

where $\theta = 45^\circ$, $V_{ac} = V_{pp} \sin \theta$, and V_{pp} is peak-to-peak voltage. I_{ac} and I_c are the amplitude of the modulated light intensity and half of the maximum intensity of the output laser, respectively.

Using this method, we determined that the EO coefficient of the 4AMP-I crystal is 1–2 pm V⁻¹ and is relatively frequency-independent up to 100 kHz (Figure 3b). The bromine-doped 4AMP-Br/I crystals exhibit an effective EO coefficient of 95 pm V⁻¹ at 1 kHz, and the power of the transmitted beam increases linearly as a function of the applied AC voltage (Figure 3c). This represents a 50-fold enhancement compared to the undoped 4AMP-I crystal and is roughly 3× higher than that of LiNO₃.^[26] However, we observed a sharp drop-off in EO coefficient with an increase in frequency response, and the effective EO coefficient dropped to 42 pm V⁻¹ at 10 kHz.

Based on the frequency dependence, we hypothesized that ion migration might be playing a role. To explore this, we conducted an impedance study on the doped and undoped samples (Figure 4a). We began by measuring the impedance spectrum of LiNbO₃ as a control, since there should be no appreciable ion migration. As expected, the capacitance of LiNbO₃ does not change appreciably within the measurement frequency range of 100 Hz to 100 kHz. The impedance evolution of 4AMP-I is similar to that of LiNbO₃, where the change is negligible at higher frequencies. In contrast, the capacitance of 4AMP-Br/I drops rapidly at high frequencies, mimicking the trends observed in the EO performance. Thus, we attribute the frequency-dependent EO response of 4AMP-Br/I to ion migration, where an ion-driven, dynamic polarization adds to the intrinsic polarization (Figure 4b) of the sample.

Since HOIPs are receiving further exploration as EO materials, it will be important to continue to report studies of the frequency-dependence of their EO responses. In our own recent study of the organic perovskite (DCl)(NH₄)(BF₄)₃, we achieved ≈20 pm V⁻¹ by increasing the dipole moment of the A-site cation.^[10] Its performance is higher than that of the less polar (DH)(NH₄)(BF₄)₃, but to achieve wide applicability, such materials will ideally sustain high responses well beyond the 1 kHz reported in that study, and thus require explicit measurement and reporting over this wider regime of frequency response.

3. Conclusion

In summary, we report a frequency-dependent EO response in halide-mixed quasi-2D perovskite crystals. With a small amount of Br- ($x = 6.7\%$) doped into the X-site, 4AMP-Br/I crystals exhibit an effective EO coefficient of 95 pm V⁻¹ at 1 kHz. However, this drops rapidly with increasing frequency. By correlating EO performance with impedance measurements, we determined that the large EO response originates largely from ion migration, which adds a slow-response, dynamic polarization. These findings highlight the impact that ion migration can have on EO measurements and suggest that impedance spectroscopy can help determine its presence in future studies.

4. Experimental Section

Material synthesis: 4-(aminomethyl)piperidinium iodide (4AMP-2HI). An HI aqueous solution (57 wt%, 50 mmol) was added dropwise to a solution of 4-piperidinethanamine (20 mmol) in methanol (10 mL) at 0 °C. The solution was stirred at 0 °C for 3 h. Then a large amount of diethyl ether was added into the solution. The precipitation was collected by centrifugation and recrystallized with acetone and diethyl ether, affording 4-(aminomethyl)piperidinium iodide as white crystal (yields ≈80%). (4AMP)(MA)₂Pb₂I₇ crystals were prepared by adopting the step-cooling method. Briefly, the molar ratios of 4AMP-2HI: MAI: PbI₂ are 0.15:1:1. 4AMP-2HI, MAI and PbI₂ were dissolved in 3 mL of hydroiodic acid and 0.3 mL of hypophosphorous acid solution by heating under stirring for 10–20 min at ≈130 °C, until the solution turned clear yellow. The solution was kept at 130 °C for 2 h and then was cooled to room temperature at a rate of 1 °C h⁻¹ to yield centimeter-sized red crystals. The (4AMP)(MA)₂Pb₂(Br_{*x*}/I_{*1-x*})₇ ($x = 6.7\%$) crystal was prepared in a similar way, using HI and HBr mixed solution ($V_{HI}/V_{HBr} = 2/1$) instead of HI solution.

Density Functional Theory: The polarization calculations were performed using CP2K.^[27,28,29] An energy cutoff of 600 Ry was set for Gaussian basis sets with auxiliary planewave method. Geometry optimization was performed under Broyden–Fletcher–Goldfarb–Shanno algorithm. Berry phase approach was utilized to calculate system electric polarization.^[30] The configurations of Br/I mixed perovskites are determined using the site-occupancy disorder code.^[31]

Characterization: Powder XRD patterns were collected using a Rigaku MiniFlex 600 diffractometer equipped with an NaI scintillation counter and using monochromatized Cu K α radiation ($\lambda = 1.5406 \text{ \AA}$). For SHG measurements, a 1030 nm fundamental (5 kHz) was produced by an ytterbium-doped potassium gadolinium tungstate regenerative amplifier

(Pharos, Light Conversion). The beam was then sent through an optical parametric amplifier (Orpheus, Light Conversion), to generate the wavelengths 1510, 1530, and 1550 nm. Scattered light from the powders was then collected through two lenses into a 400 μm multimode fiber (Thorlabs), which was sent to a USB2000+ spectrometer (Ocean Optics). Angle-resolved Raman measurements were carried out with an inVia Confocal Raman system (Renishaw), in conjunction with a 785 nm single-mode laser (IPS). Samples were placed on a microscope slide, which was held onto a Thorlabs rotation stage. XPS measurements were performed with the Thermo Scientific K-Alpha system with Al K α source. The takeoff angle used was 90°. The impedance spectrum was measured using a potentiostat electrochemical workstation (AUT50690, PGSTAT204, The Netherlands) at different biases. The frequency ranged from 100 kHz to 100 Hz.

Supporting Information

Supporting Information is available from the Wiley Online Library or from the author.

Acknowledgements

M.-J.S. and R.S. contributed equally to this work. This work was financially supported by Huawei Technologies Canada Co., Ltd. and the Natural Sciences and Engineering Research Council (NSERC). Computations were performed on the Niagara supercomputer at the SciNet HPC Consortium. SciNet is funded by: the Canada Foundation for Innovation; the Government of Ontario; Ontario Research Fund-Research Excellence; and the University of Toronto.

Conflict of Interest

The authors declare no conflict of interest.

Data Availability Statement

The data that support the findings of this study are available from the corresponding author upon reasonable request.

Keywords

electro-optics, ion migration, quasi-2D perovskites, spontaneous polarization

Received: August 10, 2021
Revised: September 21, 2021
Published online:

- [1] C. Wang, M. Zhang, X. Chen, M. Bertrand, A. Shams-Ansari, S. Chandrasekhar, P. Winzer, M. Lončar, *Nature* **2018**, 562, 101.
- [2] A. D. Dupuy, Y. Kodera, J. E. Garay, *Adv. Mater.* **2016**, 28, 7970.
- [3] L. R. Dalton, P. A. Sullivan, D. H. Bale, *Chem. Rev.* **2010**, 110, 25.
- [4] B. Saparov, D. B. Mitzi, *Chem. Rev.* **2016**, 116, 4558.
- [5] Y. Gao, G. Walters, Y. Qin, B. Chen, Y. Min, A. Seifitokaldani, B. Sun, P. Todorovic, M. I. Saidaminov, A. Lough, S. Tongay, S. Hoogland, E. H. Sargent, *Adv. Mater.* **2019**, 31, 1808336.
- [6] a) Y. Ai, X.-G. Chen, P.-P. Shi, Y.-Y. Tang, P.-F. Li, W.-Q. Liao, R.-G. Xiong, *J. Am. Chem. Soc.* **2019**, 141, 4474; b) H.-Y. Zhang, X.-J. Song, X.-G. Chen, Z.-X. Zhang, Y.-M. You, Y.-Y. Tang, R.-G. Xiong, *J. Am. Chem. Soc.* **2020**, 142, 4925; c) C.-R. Huang, X. Luo, X.-G. Chen, X.-J. Song, Z.-X. Zhang, R.-G. Xiong, *Natl. Sci. Rev.* **2021**, 8, nwa232.
- [7] a) G. Long, R. Sabatini, M. I. Saidaminov, G. Lakhwani, A. Rasmita, X. Liu, E. H. Sargent, W. Gao, *Nat. Rev. Mater.* **2020**, 5, 423; b) C.-K. Yang, W.-N. Chen, Y.-T. Ding, J. Wang, Y. Rao, W.-Q. Liao, Y.-Y. Tang, P.-F. Li, Z.-X. Wang, R.-G. Xiong, *Adv. Mater.* **2019**, 31, 1808088.
- [8] M. I. Saidaminov, O. F. Mohammed, O. M. Bakr, *ACS Energy Lett.* **2017**, 2, 889.
- [9] Y. Gao, S. Meshkat, A. Johnston, C. Zheng, G. Walters, Q. Feng, X. Wang, M.-J. Sun, A. M. Najarian, D. Xue, Y.-K. Wang, M. I. Saidaminov, O. Voznyy, S. Hoogland, E. H. Sargent, *ACS Appl. Mater. Interfaces* **2021**, 13, 19042.
- [10] M.-J. Sun, C. Zheng, Y. Gao, A. Johnston, A. M. Najarian, P.-X. Wang, O. Voznyy, S. Hoogland, E. H. Sargent, *Adv. Mater.* **2021**, 33, 2006368.
- [11] L. Protesescu, S. Yakunin, M. I. Bodnarchuk, F. Krieg, R. Caputo, C. H. Hendon, R. X. Yang, A. Walsh, M. V. Kovalenko, *Nano Lett.* **2015**, 15, 3692.
- [12] M. Daub, H. Hillebrecht, *Angew. Chem., Int. Ed.* **2015**, 54, 11016.
- [13] E. T. Hoke, D. J. Slotcavage, E. R. Dohner, A. R. Bowring, H. I. Karunadasa, M. D. McGehee, *Chem. Sci.* **2015**, 6, 613.
- [14] W. Mao, C. R. Hall, S. Bernardi, Y.-B. Cheng, A. Widmer-Cooper, T. A. Smith, U. Bach, *Nat. Mater.* **2021**, 20, 55.
- [15] J. Mizusaki, K. Arai, K. Fueki, *Solid State Ionics* **1983**, 11, 203.
- [16] H. J. Snaith, A. Abate, J. M. Ball, G. E. Eperon, T. Leijtens, N. K. Noel, S. D. Stranks, J. T.-W. Wang, K. Wojciechowski, W. Zhang, *J. Phys. Chem. Lett.* **2014**, 5, 1511.
- [17] Y. Yuan, J. Huang, *Acc. Chem. Res.* **2016**, 49, 286.
- [18] T. Cheng, G. Tumen-Ulzii, D. Klotz, S. Watanabe, T. Matsushima, C. Adachi, *ACS Appl. Mater. Interfaces* **2020**, 12, 33004.
- [19] M. Karlsson, Z. Yi, S. Reichert, X. Luo, W. Lin, Z. Zhang, C. Bao, R. Zhang, S. Bai, G. Zheng, P. Teng, L. Duan, Y. Lu, K. Zheng, T. Pullerits, C. Deibel, W. Xu, R. Friend, F. Gao, *Nat. Commun.* **2021**, 12, 361.
- [20] a) T. Wu, M. Ahmadi, B. Hu, *J. Mater. Chem. C* **2018**, 6, 8042; b) X. Y. Chin, D. Cortecchia, J. Yin, A. Bruno, C. Soci, *Nat. Commun.* **2015**, 6, 7383.
- [21] D. Zhang, Z.-D. Luo, Y. Yao, P. Schoenherr, C. Sha, Y. Pan, P. Sharma, M. Alexe, J. Seidel, *Nano Lett.* **2021**, 21, 995.
- [22] a) L. Mao, W. Ke, L. Pedesseau, Y. Wu, C. Katan, J. Even, M. R. Wasielewski, C. C. Stoumpos, M. G. Kanatzidis, *J. Am. Chem. Soc.* **2018**, 140, 3775; b) L. N. Kantorovich, I. I. Tupitsyn, *J. Phys.: Condens. Matter* **1999**, 11, 6159.
- [23] C. C. Teng, H. T. Man, *Appl. Phys. Lett.* **1990**, 56, 1734.
- [24] P. M. Lundquist, M. Jurich, J. F. Wang, H. Zhou, T. J. Marks, G. K. Wong, *Appl. Phys. Lett.* **1996**, 69, 901.
- [25] B. Liu, C. M. M. Soe, C. C. Stoumpos, W. Nie, H. Tsai, K. Lim, A. D. Mohite, M. G. Kanatzidis, T. J. Marks, K. D. Singer, *Sol. RRL* **2017**, 1, 1700062.
- [26] Y. Shuto, M. Amano, *J. Appl. Phys.* **1995**, 77, 4632.
- [27] J. Hutter, M. Iannuzzi, F. Schiffmann, J. VandeVondele, *Wiley Interdiscip. Rev.: Comput. Mol. Sci.* **2014**, 4, 15.
- [28] B. G. Lippert, J. H. Parrinello, M. Parrinello, *Mol. Phys.* **1997**, 92, 477.
- [29] J. VandeVondele, M. Krack, F. Mohamed, M. Parrinello, T. Schassaing, J. Hutter, *Comput. Phys. Commun.* **2005**, 167, 103.
- [30] S. Lubser, *J. Chem. Phys.* **2014**, 141, 234110.
- [31] R. Grau-Crespo, S. Hamad, C. R. A. Catlow, N. H. de Leeuw, *J. Phys.: Condens. Matter* **2007**, 19, 256201.